

Section 2

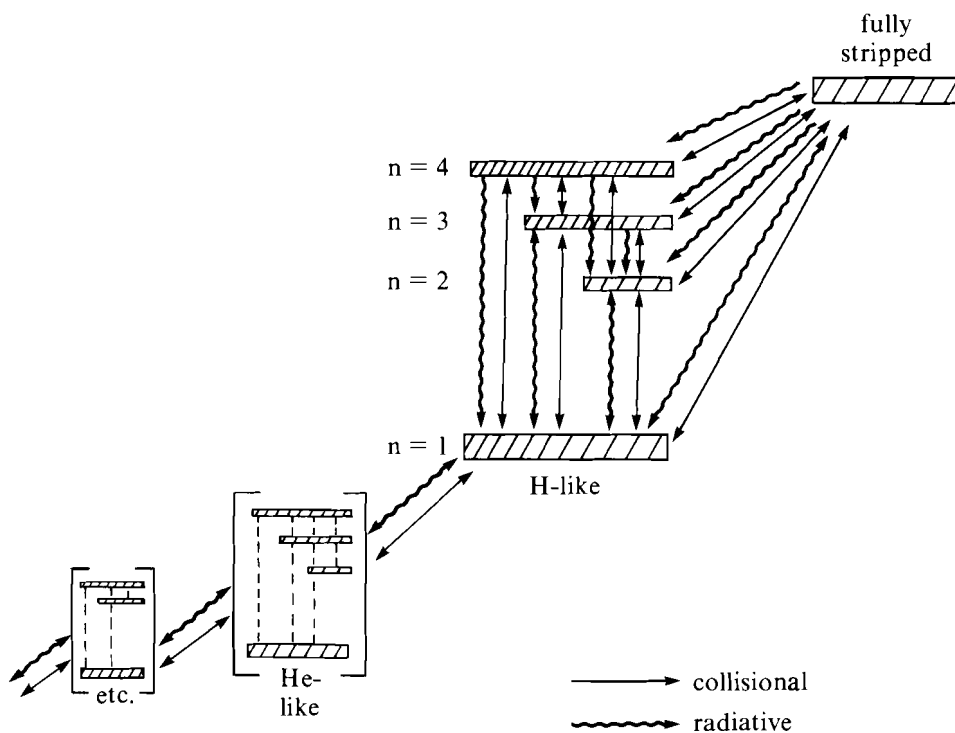
ADVANCED TECHNOLOGY DEVELOPMENTS

2.A The Design And Optimization of Recombination X-Ray Lasers

This article explores a number of theoretical issues crucial to the understanding and design of extreme-ultraviolet (XUV) recombination lasers. Our interest in this area was sparked by strong evidence that the Balmer- α line of hydrogen-like carbon at 182.3 Å was being amplified in plasmas produced in a series of exploding-foil experiments performed on OMEGA.¹ The targets consisted of a Formvar (polyvinyl formal, C₁₁H₁₈O₅) layer, which contains the carbon, and a selenium layer. The laser action was the result of recombination onto fully stripped ions of carbon.

The original goal of this experiment was to duplicate results obtained at the Lawrence Livermore National Laboratory, where amplification of fine-structure transitions of neon-like selenium was observed.² Consequently, the result indicating amplification of the carbon line was surprising, and it drew a prompt reaction from Nam *et al.*, who attributed the unexpected recombination behavior to rapid radiational cooling of the Formvar plasma by the selenium.³ We have recently applied our hydrodynamic, atomic, and radiative-transfer modeling capabilities to this problem, to arrive at an understanding of this experiment and to explore recombination lasing as an option for future experiments at LLE. We will show the importance of radiative cooling relative to the importance of other effects, such as cylindrical expansion and lasing purity, in optimizing experiments to give the largest gain.

A carbon recombination laser is created by exploding a strip or fiber⁴ of carbon with a line-focused laser beam to form a fully stripped carbon plasma. The plasma must be cooled to a temperature where it can recombine and expand to an electron density that favors collisional recombination to levels of the hydrogen-like species that are at or above the top of the inversion one wishes to create. Figure 33.15 illustrates a simplified level diagram of the hydrogen-like species as it is treated in the postprocessor described below. The arrows indicate the collisional and radiative processes connecting the various levels included in the atomic model. We seek to feed the levels above the $n=2$ level so that an inversion forms between the $n=3$ and $n=2$ levels of the Lyman- β transition. Lyman- α emission from the $n=2$ to $n=1$ transition depletes the lower level and deepens the inversion. On the other hand, the Lyman- α photons can be reabsorbed by photoexcitation of the same transition, which repopulates the $n=2$ level and destroys the inversion. Consequently, the plasma must be optically thin to this radiation. The cooling and expansion of the explosion must be rapid enough to bring the plasma to the desired range of conditions before most of the bare carbon has been recombined away.



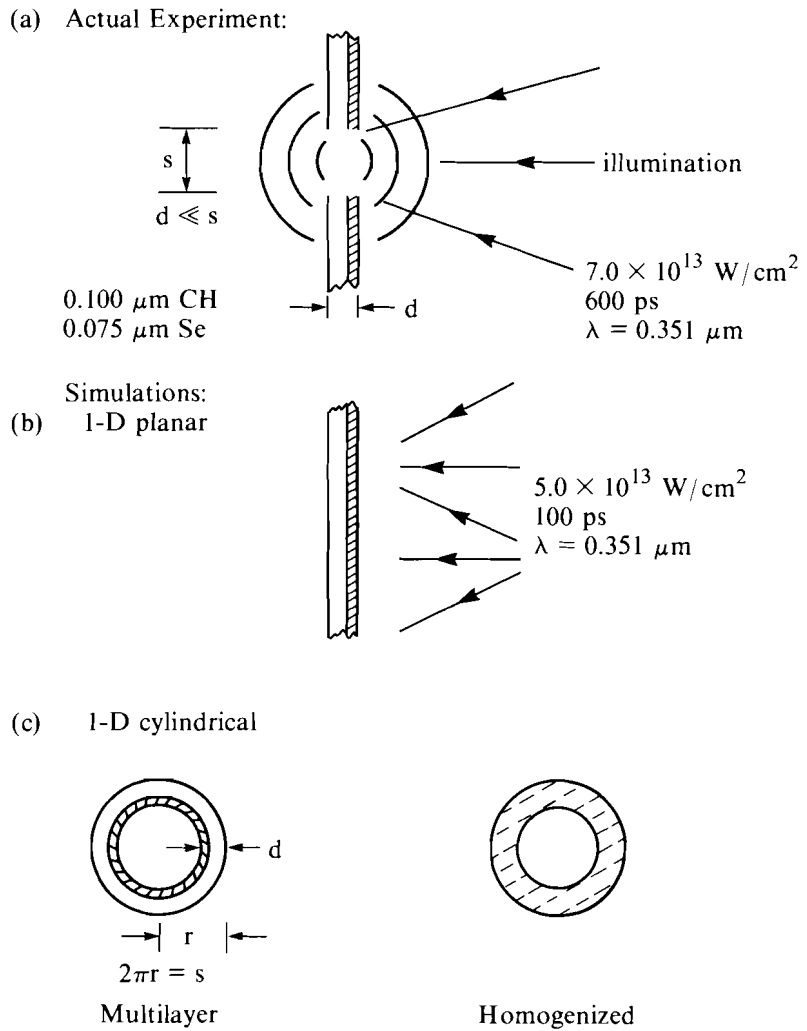
TC1478

Fig. 33.15
Rate equations. The recombination pumping mechanism in hydrogen-like carbon, illustrated here, is simulated by the ionization and level-kinetics model in the non-LTE radiation postprocessor.

Whether or not it is possible to rapidly cool a hot plasma while bringing it to the right range of density without first having the laser ions recombine away can be best answered by means of a full hydrodynamic simulation. The use of detailed modeling of laser-matter coupling and hydrodynamics in the one-dimensional hydrocode *LILAC*⁵ establishes a credible connection between favorable lasing conditions in the target plasma and plausible experimental scenarios. The simulations are based on *LILAC* running with average-ion atomic physics and a radiative-transfer postprocessor that uses a detailed-configuration model of the ionic level populations and a line-of-sight solution to the equation of transfer to model the laser action. In Nam *et al.*,³ which addresses the OMEGA experiment, the density and temperature histories are obtained from an idealized homogeneous one-zone model evolving from initial conditions that are not shown to be attainable with a real laser and target. Unlike all published simulations of similar experiments of which we are aware, we use a nonlocal model of the resonance-line photoexcitation of the lower level of the lasing transition. Emission- and absorption-line profiles are explicitly Doppler shifted according to the hydrodynamic velocity projected along the line of sight. The usual technique is to assume that the resonance emission either escapes or is reabsorbed within the zone where it originates, according to an escape probability that is calculated in terms of local plasma conditions and the local velocity divergence.⁶ Other questions beyond the reach of one-zone semi-analytic calculations concern the spatial and temporal distribution of gain or—more specifically, whether the amplifying plasma is distributed broadly through the center of the plasma, whether only a small part of the plasma participates, whether amplification occurs in different parts of the plasma at different times, the lifetime of the gain, and so on. These questions arise in determining whether a pulse of light encounters amplifying plasma along the entire length of its travel through the plasma and in answering other questions regarding the net efficiency of a laser design.

Figure 33.16(a) shows schematically the configuration of the experiment of interest. A layered target consisting of a 0.075- μm selenium layer deposited on a 0.1- μm Formvar foil backing was illuminated from the selenium side along a strip 100- μm wide at an intensity of $7.0 \times 10^{13} \text{ W/cm}^2$. Simulating this experiment in one dimension is not straightforward. A plane-parallel simulation, illustrated in Fig. 33.16(b), does not include the cylindrical divergence necessary for the expansion cooling of the plasma. To model the cylindrical divergence, simulations in cylindrical geometry, illustrated in Fig. 33.16(c), were performed. The target in this case is a cylinder made of the same layered foil as in the plane parallel case, rolled into a circumference equal to the irradiated width of the actual experiment. This results in the same amount of irradiated material per unit axial length of target and in the same irradiance on target at the original radius in the cylindrical simulation as in the actual experiment.

Two aspects of the cylindrical simulation that depart from the experiment are that the inner part of the cylinder implodes for a short time and that the target in the simulation must be homogenized



TC2151

Fig. 33.16 Target geometries for 1-D simulation of cylindrical plasmas from exploding foils. Simulations in cylindrical geometry are used to model the cylindrical divergence of the foil exploding under line-focused illumination. Mixing is modeled by homogenizing the foil materials.

initially. The implosive episode in the simulation ends relatively quickly. By the time the plasma has expanded to the range of density of interest for recombination pumping at a diameter over 200 μm , details of the plasma conditions characteristic of this episode have smoothed away. Effects due to the initial geometry on the absorption of laser energy are at the level of fine tuning that is not of interest to the principles addressed in this article. Modeling the cylindrical expansion is a far more important consideration. Homogenizing the materials anticipates the mixing that is bound to occur to some degree and also serves as a compromise that allows materials from both layers to expand. Otherwise, the layer arbitrarily chosen to be the inner layer would be confined. It will be shown below that the carbon must mix with the selenium to some extent in order for the radiative cooling to be effective.

The hydrodynamic simulations employ a non-LTE average-ion model of the atomic physics. In this model, all ions of each element in a fluid zone are represented by a single ion whose level populations are the mean level populations of all such ions.⁷ Our model includes the lowest ten principal quantum levels of each average ion. In glass, for example, the atomic description would consist of ten level populations for the average silicon ion and ten level populations for the average oxygen ion. In this manner, one can describe an arbitrary mixture of elements.

The level populations are calculated from time-dependent rate equations, including collisional ionization, recombination, excitation, and de-excitation; spontaneous emission; radiative recombination; and dielectronic recombination. The level energies are obtained using values of Slater screening coefficients⁸ obtained by R. More.⁹ Values of the rates are obtained from formulas appropriate for a screened hydrogenic approximation, where the active electron in a multi-electron ion is treated as if it were interacting only with a nucleus whose charge is determined from the nuclear charge and the effective screening of the spectator electrons, and where the multiplicities and vacancies of the participating levels are taken into account. Opacities and emissivities are calculated from the level populations. In the current version of the model, photoexcitation and photoionization are in the opacity model, but they are not coupled to the atomic rate equations. Following the example of Nam *et al.*, the emissivity due to fine-structure transitions is taken from a two-level model involving the ground state of the ion and the average of all levels representing a fine-structure excitation from the ground state.³ Energies, statistical weights, and oscillator strengths for this average fine-structure transition are taken from Post *et al.*¹⁰ The population of this average fine-structure excitation is obtained from the equilibrium between collisional excitation and decay and spontaneous emission. This contribution is expected to dominate the cooling in recombination-pumped lasing where the plasma cools to temperatures too low to excite transitions between the principal quantum levels at significant rates.

The output of the hydrodynamic simulation is fed into a postprocessor that calculates the atomic physics and radiative transport of the simulation in terms of a multispecies detailed-configuration atomic model capable of simulating the recombination pumping mechanism in the hydrogen-like species, and in terms of a line-of-sight integration of the equation of transfer capable of calculating the coupling of resonance radiation with the atomic-level populations.¹¹ This postprocessor has been upgraded to include the effects of the Doppler shift of emission and absorption line profiles on the photoexcitation rates. The hydrodynamic Doppler shift significantly increases the escape probability of carbon Lyman- α radiation, which would otherwise destroy the population inversion by populating its lower level.

A useful depiction of the behavior of an exploding carbon plasma is its trajectory in the temperature-density plane shown in Fig. 33.17(a).

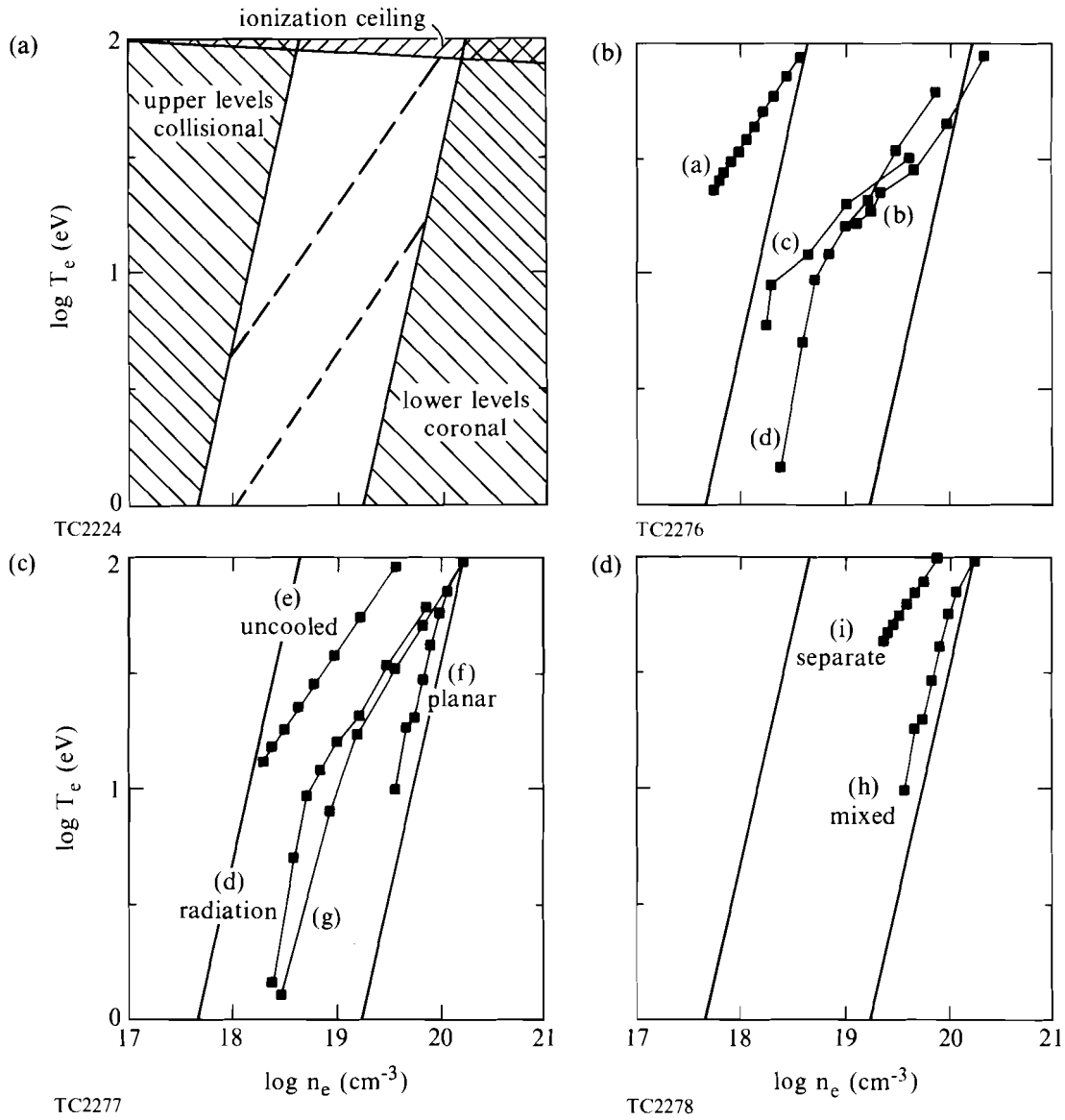


Fig. 33.17

Conditions permitting gain in the 3-to-2 transition at 182.3 Å in hydrogen-like carbon. Conditions allowing rapid recombination to the upper level of the inversion without close collisional coupling between the two inverted levels roughly define a region in the temperature-density plane where gain is expected. The overlays show trajectories of conditions obtained in various cases. Marks are placed every 200 ps. Cooling is delayed too long with a 600-ps pulse [curve (a)]. Conditions in the case of Nam *et al.* were obtained from an idealized one-zone simulation [curve (b)]. Conditions in the case of Lee and Estabrook were obtained from a hydrocode simulation of a case that gives good gain [curve (c)]. The case labeled "radiation" [curve (d)] is our example chosen to make comparisons illustrating the importance of various effects. Here, it is seen by comparison with an "uncooled" simulation [curve (e)] that radiative cooling is an important mechanism for cooling the plasma. Planar expansion does not lower the temperature quickly enough [curve (f)]. The best results were obtained from a simulation employing a pure carbon target [curve (g)]. Mixing of the lasant and coolant is required for radiative cooling to be effective [curves (h) and (i)].

From a few simple considerations, approximate limits on the useful area in the plane can be obtained. The labeled shaded areas indicate where inversion in the $n=3$ to $n=2$ interval cannot be achieved. Above the ionization ceiling, temperatures are too high for recombination to take place. To the left of the left-hand boundary, the collision rates are not high enough to have rapid recombination and rapid feeding of the upper lasing level from higher levels. To the right of the right-hand boundary, the collisional coupling of the $n=3$ to $n=2$ levels is rapid enough to destroy the inversion. The fact that collisional rates are more rapid for smaller transition and ionization energies allows an area where an inversion can be formed.

Plasmas enter this temperature-density diagram from the upper right as they expand and cool from a hotter, denser state. The optimum conditions are at temperatures below about 10 eV, where collisional excitation and collisional ionization contribute negligibly, and at electron densities slightly higher than 10^{19} cm⁻³. As for all other relevant processes, the spontaneous emission rate is constant, and collisional recombination and de-excitation at low temperatures proceed according to rate coefficients that scale as $n_e/T_e^{1/2}$. Consequently, the level-population equations are invariant below about 10 eV along lines parallel to the left and right boundaries of the "allowed" area of the diagram. At lasing conditions that are near optimum, recombination of the bare carbon species is nearly complete well within one nanosecond, so not only must the plasma trajectory arrive near the 10 eV- 10^{19} cm⁻³ point, it must arrive quickly, before the lasing supply has disappeared. The dashed lines in the diagram show the slope representing cooling of an ideal gas by adiabatic expansion. Since lines of constant collisional recombination rate fall along the steeper $n_e/T_e^{1/2}$ lines, the lasing supply must survive the passage through conditions where recombination occurs even faster than at the ideal destination. The gain coefficient is proportional to the degree of population inversion, as given by the difference in level population per unit statistical weight for the two levels in the lasing transition. The gain coefficient is also proportional to the spatial density of the lasing ions; for this reason, in addition to the above considerations, the highest gain occurs at the highest density that does not lead to collisional disruption of the inversion.

Curve (a) in Fig. 33.17(b) shows the trajectory of typical conditions in the exploding foil obtained in the simulation of the OMEGA experiment. The points on the curve are placed 200 ps apart. No gain is obtained in this plasma because it does not cool below the recombination ceiling until after it has expanded beyond the range of useful densities. This delay results from using too long a laser pulse because cooling cannot begin until after the pulse ends, even if the plasma has expanded below the critical density for the illumination wavelength.¹²

The observation of gain in an exploding-foil target under irradiation as long as 600 ps is a mystery at this time. There is no indication that pulses this long could ever allow the exploded foil to cool quickly enough. On the other hand, shorter pulses of 100 ps, for example, can

produce amplifying plasmas, which tempts speculation that some unanticipated diversion of the laser illumination away from the plasma could have allowed the plasma to cool. We will not delve further into exotic explanations that we can neither substantiate nor rule out. Instead, we leave this problem as an interesting puzzle for future work and confine our attention to illumination pulses of 100 ps and to simulations that do produce gain.

An optimized case obtained by Nam *et al.*³ is represented by the trajectory [curve (b)] [Fig. 33.17(b)], again with points placed 200 ps apart. These conditions do produce gain, in contrast to the conditions in curve (a) [Fig. 33.17(b)], but because they represent a one-zone model of a plasma expanding from an ad hoc initial configuration, there remains the question of whether they can be duplicated in a more realistic simulation of a plasma exploded from a foil by a laser. Qualitatively, this trajectory is a typical favorable case. The density drops quickly into the favorable area so that the loss of bare carbon is minimal. Even though radiative cooling is comparable to expansion cooling in this plasma, the trajectory remains roughly parallel to the adiabatic slope. Presumably, radiative losses are countered by the electron binding energy released by collisional recombination and decay. Another favorable trajectory [curve (c)], shown in Fig. 33.17(b), represents a single Lagrangian zone in the plasma ablated off the surface of a carbon fiber simulated by Lee and Estabrook using a hydrocode.¹³ It is interesting that the two trajectories show a similarity not only to each other, but to that of our chosen example, shown in Fig. 33.17(b) [curve (d)].

Figure 33.17(c) shows by comparison the effect of radiative cooling on one case simulated on *LILAC*. The case labeled “radiation” is the standard case given by curve (d) in Fig. 33.17(b). This simulation employs a foil 0.175- μm thick, composed of the same thicknesses of CH and selenium as in the original OMEGA experiment, homogenized and rolled into a cylinder 15.9 μm in radius. The UV (0.351- μm) illumination has been reduced to 5.0×10^{13} W/cm² at a pulse length of 100 ps. The plotted conditions are taken from the history of one of the Lagrangian zones near the center of the foil where gain was obtained. Comparison of the “radiation” and “uncooled” trajectories shows that the desired higher density results from the additional cooling. The trajectory labeled “uncooled” [curve (e)] represents the same length of time as the standard case, but it follows an ideal-gas adiabat, while the standard case eventually falls more rapidly and more steeply as radiative cooling overtakes the adiabatic cooling. In this case, at least, it is clear that radiative cooling can be a useful device for shaping the trajectory. While under conditions that permit gain due to recombination pumping, any lowering of the temperature reduces collisional excitation and ionization rates relative to the pumping rates and also reduces the pressure that drives the plasma to lower densities where the pumping rates and the laser ion density are lower.

Curve (f) in Fig. 33.17(c) shows the plane-parallel counterpart of the standard case illustrated in curve (d). The comparison shows that cylindrical expansion is the dominant cooling mechanism, even in the

presence of radiative cooling, and that planar expansion is not nearly as effective. The “planar” trajectory moves into a region of good conditions for gain, but cooling is too slow to keep the laser from being depleted by recombination.

Figure 33.17(d) shows a comparison of trajectories for two plane-parallel simulations. The “mixed” case [curve (h)] is the same as the standard case, except that the foil is unrolled and the one-dimensional simulation geometry is planar. The companion “separate” case [curve (i)] is identical, except that the selenium and plastic are separated as in the original experiment. Both trajectories are relatively slow because planar expansion is not as fast as cylindrical expansion. In the mixed case, radiative cooling pulls the trajectory down from the adiabat. In the separate case, the trajectory for a central zone in the CH layer is very nearly adiabatic. Even though there is radiative cooling in the selenium, the thermal contact with the carbon-containing layer is not effective. This shows that mixing is essential if radiative cooling is to work under the conditions of interest.

Curve (g) in Fig. 33.17(c) shows the trajectory for a case that yields the highest gain obtained in our calculations. Details of this simulation are given below. The expansion is very rapid, and the cooling is slightly faster than adiabatic. The cylinder is made of pure carbon and has half the radius of the standard case so that the rate of relative expansion is more rapid.

In the standard case, gain occurs in a cylindrical region starting about $300\ \mu\text{m}$ from the center of the plasma about 840 ps after the peak of the pulse, or at 1.0 ns into the simulation as shown in Fig. 33.18(a). The points represent individual Lagrangian zones. The gain profiles rise at this radius and then spread outward. Figure 33.18(b) shows the results of a calculation identical in every respect, except that the pumping of the lower level due to absorption of the Lyman- α emission of hydrogen-like carbon is neglected. Comparison of the two figures provides a good illustration of the damaging effects of photoexcitation. The results, including photoexcitation, are almost identical with the results ignoring this effect, except that additional expansion is needed to raise the Lyman- α escape probability. This can be observed more easily in Fig. 33.19, where the gain profiles are seen to become very nearly the same after 1.4 ns. This behavior is similar to that obtained using local escape probability approximations.³ It is significant that a nonlocal treatment gives similar results. Even though the local and nonlocal models are quite different, the differences would affect the results under conditions intermediate between those giving certain capture and certain escape. In this case, the plasma passes through the intermediate state quickly enough for the differences to escape notice.

Figure 33.20 shows that significant improvement can be obtained by reducing the amount of cylinder material, the carbon in particular, so that the plasma need not expand as far to become optically thin to the carbon Lyman- α . By removing the hydrogen, leaving a carbon/selenium mixture, the spatial density of carbon at the lasing density is increased slightly, which also increases the gain.

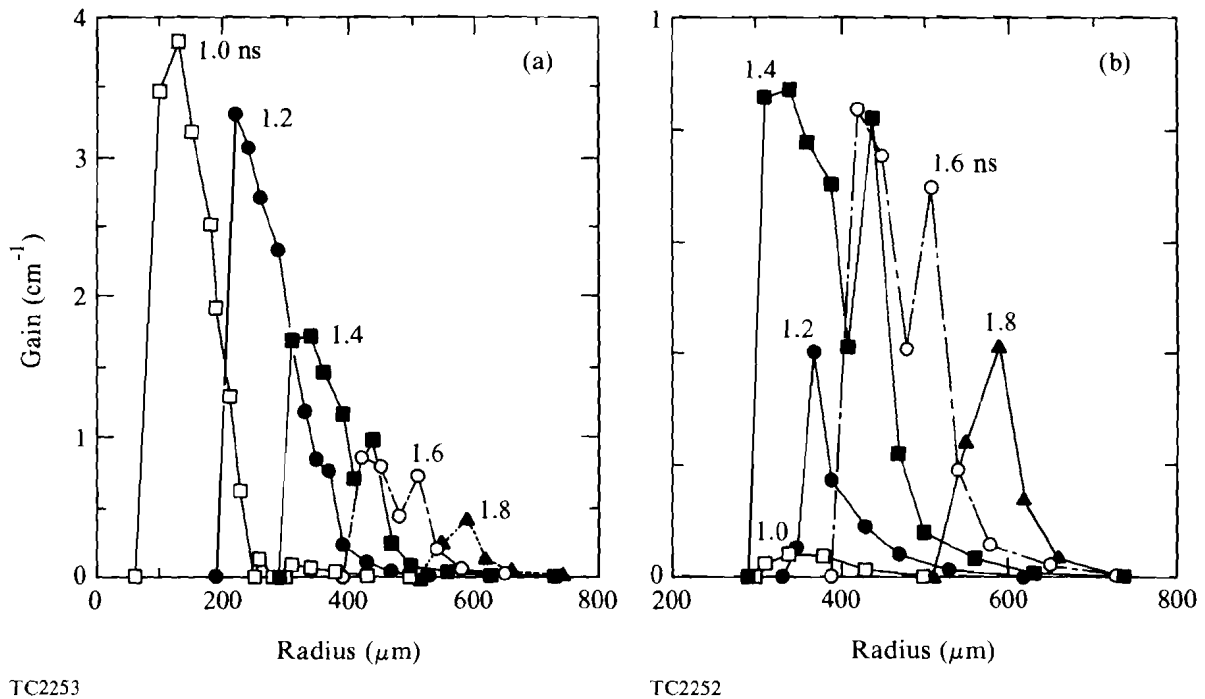


Fig. 33.18

- (a) Profiles of gain at 182.3 \AA in an exploding CH/Se cylinder; free escape. Gain occurs in a fairly narrow region that moves through the plasma.
- (b) Profiles of gain at 182.3 \AA in an exploding CH/Se cylinder; Doppler-assisted escape. Radiative capture of carbon Lyman- α reduces the gain at earlier times.

Carrying the optimization one step further, we obtain the very much improved gain profiles shown in Fig. 33.21. The trajectory for this simulation is shown as curve (g) in Fig. 33.17(c).

The target has been reduced to a thickness of $0.045 \mu\text{m}$ and a radius of $8.0 \mu\text{m}$. The target is pure carbon, with no coolant. A greatly reduced driver intensity of 0.05 TW/cm is permitted. What is particularly interesting about this simulation is that the gain peaks simultaneously throughout the entire plasma, rather than in a wave, as in the previous cases. The net amplification by a laser is dependent on the shape of the gain profile, and the possible advantages of having gain peak simultaneously throughout the plasma would be an interesting question to pursue. This particular target is probably too frail to construct, but it illustrates how far the optimization can be taken. A more realistic target from the fabrication standpoint is a solid fiber of roughly this diameter.^{4,13} Ideally, one would form a plasma such as this by ablating a thin layer off the fiber, leaving most of the original target behind.¹⁴

The high gain of this last case, illustrated in Fig. 33.21, can be attributed in part to the fact that the foil is pure carbon. Removing the selenium entirely defeats the radiative cooling, but increases the carbon density roughly threefold under the lasing conditions because the selenium had been contributing almost four times as many free electrons per ion as the carbon.

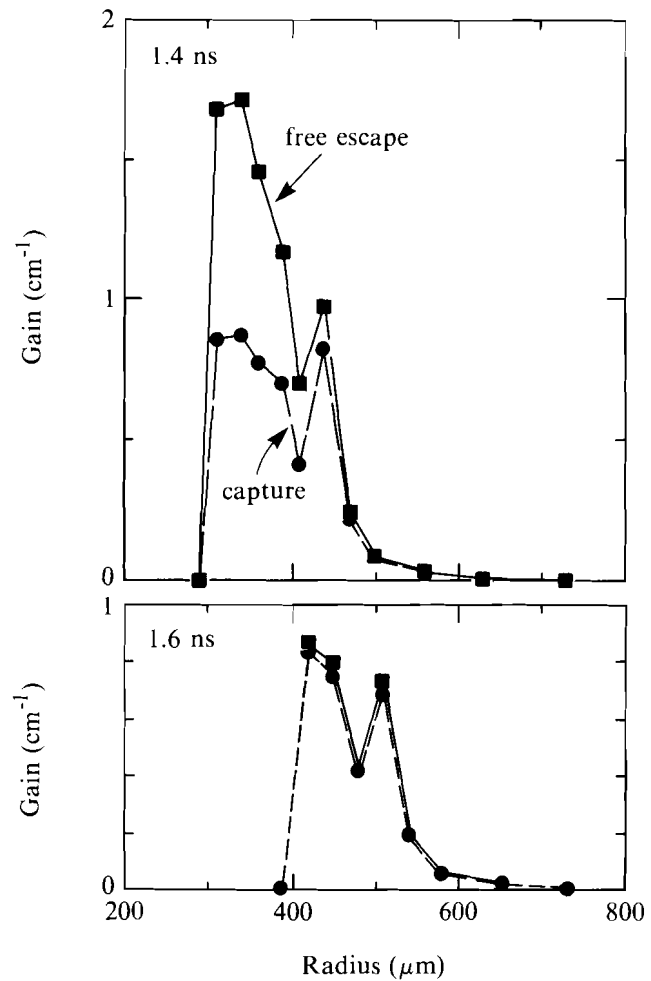
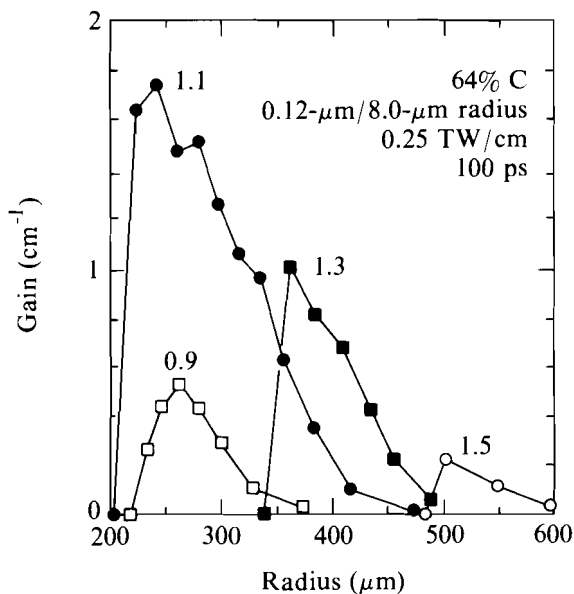


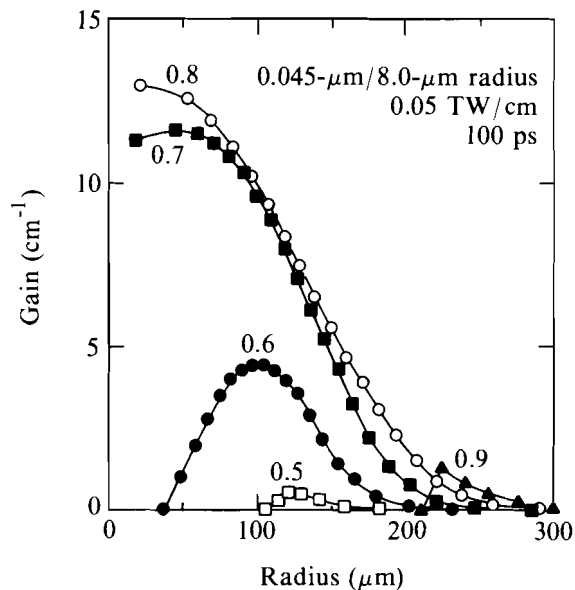
Fig. 33.19
 Profiles of gain at 182.3 Å in an exploding CH/Se cylinder. The effect of radiative capture on gain is negligible at later times.

TC2254

While much has been shown about what affects the performance of carbon XUV lasers, the observed evidence for gain using 600-ps pulses from OMEGA on foil targets remains a puzzle. Perhaps there is a means by which the illumination becomes ineffective after a much shorter time. Lasing driven by 100-ps illumination has been modeled, and it is clear that cylindrical expansion is the most important cooling mechanism. Cooling by a radiating impurity does work if it is mixed with the carbon, but diluting the lasant can reduce the gain coefficient significantly. No new behavior was obtained by using an explicit, nonlocal treatment of photoexcitation. For exploding plasmas of the kind considered here, models of photon-escape probability based on local conditions and on the local value of the velocity divergence are adequate. The transition from strong photon confinement to certain escape is rapid in both local and nonlocal treatments, so the distinctions are not important. Nevertheless, as the optical depth of the expanding plasma drops, there is a period of time where photon paths



TC2268



TC2272

Fig. 33.20 (left)

Profiles of gain at 182.3 Å in an exploding C/Se cylinder. Gain is increased by removing the hydrogen, which dilutes the lasant and does not contribute to radiative cooling, and by decreasing the mass per length of the plasma, which increases the escape probability of the carbon Lyman- α radiation.

are no longer short, compared to the plasma size, but where escape is still unlikely. Under such conditions, a local approximation does not apply, and it becomes appropriate to adopt a nonlocal model such as has been done here.

ACKNOWLEDGMENT

This work was supported by the Naval Research Laboratory under contract No. N0014-86-C-2281.

Fig. 33.21 (right)

Profiles of gain at 182.3 Å in an exploding carbon cylinder. Gain is greatly increased by removing the selenium entirely. This defeats the radiative cooling, but increases the carbon density roughly threefold under the lasing conditions because the selenium had been contributing almost four times as many free electrons per ion as the carbon.

REFERENCES

1. J. F. Seely, C. M. Brown, U. Feldman, M. C. Richardson, B. Yaakobi, and W. E. Behring, *Opt. Commun.* **54**, 289 (1985).
2. D. L. Matthews *et al.*, *Phys. Rev. Lett.* **54**, 110 (1985); M. D. Rosen *et al.*, *ibid.* **54**, 106 (1985).
3. C. H. Nam, E. Valeo, S. Suckewer, and U. Feldman, *J. Opt. Soc. Am. B* **3**, 1199 (1986).
4. G. J. Pert, *J. Phys. B* **9**, 3301 (1976).
5. An earlier version of *LILAC* is described in Laboratory for Laser Energetics Report No. 16, 1976.
6. V. V. Sobolev, *Astron. Zh. Sov. Astron.* **24**, 13 (1947), cited in V. A. Ambartsumian, *Theoretical Astrophysics* (Pergamon, New York, 1958), p. 490.
7. W. A. Lokke and W. A. Grasberger, Lawrence Livermore National Laboratory Report No. UCRL-52276, 1977 (unpublished).